ACS Photonics

pubs.acs.org/journal/apchd5

Article

Efficiently Controlling near-Field Wavefronts via Designer Metasurfaces

Weikang Pan,[#] Zhuo Wang,[#] Yizhen Chen, Xiaoying Zheng, Shiqing Li, Xinzhang Tian, Qiong He, Lei Zhou,* and Shulin Sun*

Cite This: *ACS Photonics* 2023, 10, 2423−2431

Read Online

ACCESS | Metrics & More | Article Recommendations | Supporting Information

ABSTRACT: Freely tailoring the wavefronts of surface waves (SWs) plays a vital role in on-chip photonics applications, but diffraction-optics based devices usually exhibit limited tuning functionalities and low working efficiencies. Here, we propose a new strategy to manipulate the near-field wavefronts of SWs with Pancharatnam−Berry (PB) metasurfaces exhibiting predesigned phase profiles. As a SW beam flows across such a metasurface, waves scattered by different PB meta-atoms interfere with each other, forming a new SW wavefront under appropriate wavevector matching condition. As a proof of concept, we design and fabricate a series of PB metasurfaces working in the microwave regime and experimentally demonstrate that they can efficiently realize SW manipulations, including deflection, focusing, Bessel beam, and Airy beam generations. These findings may inspire the realization of highly miniaturized on-chip devices for integrated photonics applications.

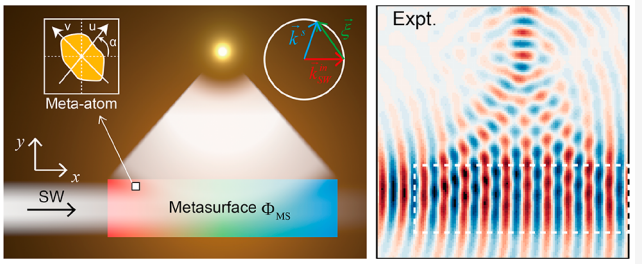

KEYWORDS: *surface waves, wavefront manipulations, metasurfaces, Pancharatnam−Berry phase, wavevector matching condition*

INTRODUCTION

Surface waves (SWs), including surface plasmon polaritons (SPPs) and spoof SPPs, are eigen electromagnetic (EM) modes tightly bound at certain interfaces between different media.[1−3] Owing to their fascinating characteristics of subwavelength resolution and local-field enhancement, SWs can be utilized to realize many on-chip photonics applications, including sub-diffraction-limited imaging,[4,5] sensing,[6−8] plasmonic laser,[9−11] on-chip plasmonic circuit,[12−14] enhanced nonlinear optics,[15−17] and so on. Manipulating SWs at will is crucial to achieve these applications and is the key aim for many frontier research.

Conventional optical elements (e.g., micro prisms, lenses, etc.) can manipulate SWs based on modulating the mode index of SWs flowing through them.[18,19] However, such devices are usually bulky in size, making them unfavorable for integration-optics applications. Bragg devices, usually composed of subwavelength grooves or slit arrays on surfaces of certain plasmonic metals,[20−24] were recently proposed to control the in-plane propagation of SWs flowing on the plasmonic surfaces. In particular, arranging such nanoarrays in certain nonperiodic manners, the resulting inhomogeneous Bragg devices can even be employed to reconstruct SW beams with complicated wavefronts, leading to fascinating effects such as SW deflection,[20] Airy beam,[21] collimated beam generations[22] and focusing,[23,24] etc. However, these Bragg devices that rely on coherent interferences of waves scattered by nanostructures arranged periodically or quasi-periodically, will inherently suffer from several limitations, such as wavelength-scale control, multimode generations, and quasi wavevector (or phase) matching, as schematically shown in Figure 1a (see numerical demonstrations in section A of the Supporting Information).

Metasurfaces, planar metamaterials composed of subwavelength microstructures (i.e., meta-atoms) arranged in certain sequences with tailored responses to impinging EM waves, were recently proposed to manipulate both propagating waves (PWs)[25] and SWs.[26] Different from the Bragg devices previously studied, metasurfaces can freely control EM waves at the deep-subwavelength scale, based on interferences of waves scattered by meta-atoms with subwavelength sizes. As the result, wave controls based on metasurfaces can resolve many issues encountered by Bragg devices, such as multimode generation and quasi wavevector matching. A series of meta-devices, composed of nanoslits[27−30] or meta-atoms[26,31−41] with more sophisticated functionalities, were recently constructed to couple PWs into SWs with desired wavefronts. However, all these meta-devices still need the illuminations of PWs, which are not convenient for those application scenarios requiring direct control on in-plane SWs.

Special Issue: Photonics in China

Received: December 27, 2022
Published: February 22, 2023

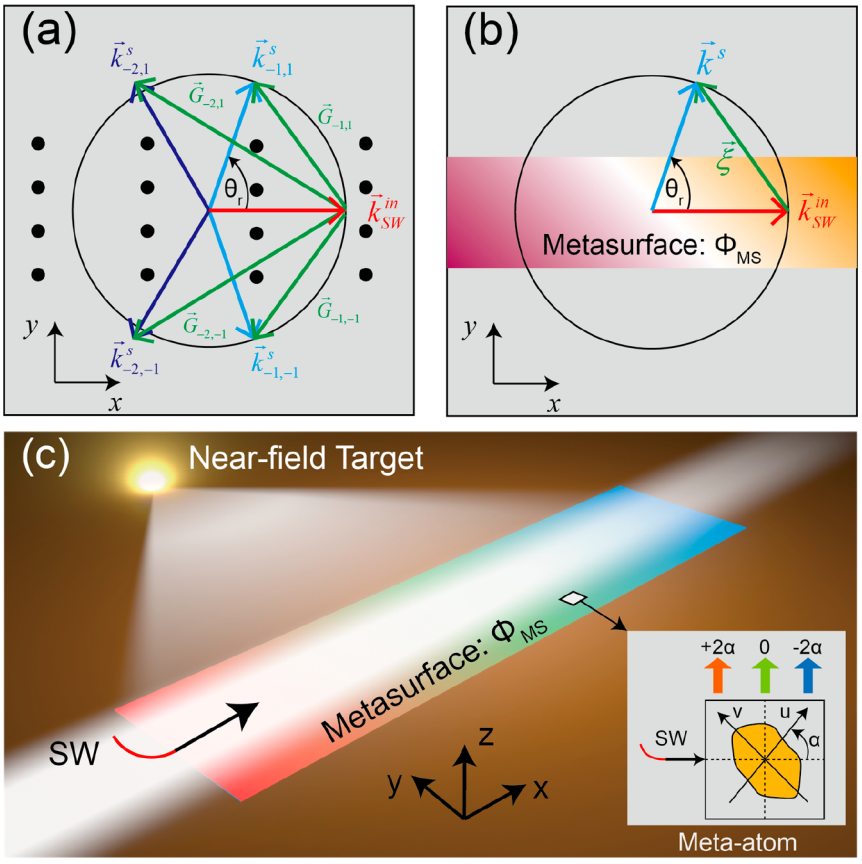

Figure 1. Scheme of SW wavefront tailoring. (a) Physical concept of SW in-plane scattering with Bragg devices. After obtaining different ordered reciprocal lattice vectors $\vec{G}_{m,n}$, the impinging SWs will be scattered to different directions in the 2D plane. (b) Proposed scheme of SW in-plane scattering with a gradient metasurface. Through providing a unique phase gradient ($\vec{\xi} = \nabla\Phi$), the metasurface will efficiently scatter the impinging SWs to the predefined direction. (c) Arbitrary SW wavefront reshaping with a gradient metasurface with a spatially varying phase gradient. As schematically shown in the inset, a normal mode carrying no geometric phase and two anomaly modes carrying opposite geometric phases will be excited by the meta-atoms under the excitation of SWs, in which only one of the abnormal modes can form the desired SW wavefront governed by the perfect wavevector matching condition.

In this Article, we propose a new strategy to directly manipulate the wavefronts of SWs following on plasmonic surfaces with carefully designed metasurfaces. As a SW beam passes through the metasurface, meta-atoms inside the device can scatter SWs with predesigned amplitudes and phases, and the interferences of these scattered waves can form a new wavefront for the SW under the wavevector matching condition (see Figure 1c). As a proof-of-concept, we design and fabricate a series of meta-devices working in the microwave regime and experimentally demonstrate various SW-manipulation effects based on these devices, including bending and focusing of SWs, and the formation of special SW beams such as Bessel and Airy beams. Full wave simulations are in nice agreement with our measurements, which collectively validate our theoretical predictions. Compared to conventional SW-manipulation devices based on geometric optics or Bragg scatterings, our metasurface-based SW-control devices exhibit the advantages of single-mode operation, high efficiency, easy integration, and possession of more diversified functionalities.

PHYSICAL CONCEPT AND META-ATOM DESIGN

We start by describing the working principle of our in-plane SW manipulations based on PB metasurfaces. As schematically shown in Figure 1b,c, as a SW beam flows across the metasurface, all meta-atoms will be excited and then radiate as subsources, with phase shifts dictated by their orientation angles according to the PB phase mechanism. Interferences of these scattered waves then form a new wavefront for the SW, determined by the phase profile encoded. In principle, the local parallel component of the electric field $\vec{E}_{\parallel}$ exciting a certain meta-atom is inhomogeneous in space, and thus, its interaction with the meta-atom is complicated. Fortunately, each meta-atom usually possesses a deep-subwavelength size, thus, we can approximately view such an inhomogeneous local field carried by the SW as a homogeneous one.[42] Under this approximation, radiation of the PB meta-atom is identical to that of the meta-atom excited by a normally incident PW with linear polarization. According to refs 43 and 44, as shined by a linearly polarized wave that can be decomposed to two circularly polarized waves with opposite helicity, the wave scattered by the meta-atom generally contains a normal mode exhibiting a linear polarization without any additional phase shift and two circularly polarized modes exhibiting opposite spin σ (σ = 1: left circular polarization; $\sigma = -1$: right circular polarization) and opposite geometric phases $\Phi^{\sigma} = \sigma 2\alpha$, in which α is the orientation angle of the meta-atom. Obviously, the normal mode is useless to reconstruct the wavefronts of SWs since they do not carry additional phases. While two abnormal SW modes carry the opposite phase gradient, only one of them carrying a specific

https://doi.org/10.1021/acsphotonics.2c02009
ACS Photonics 2023, 10, 2423−2431

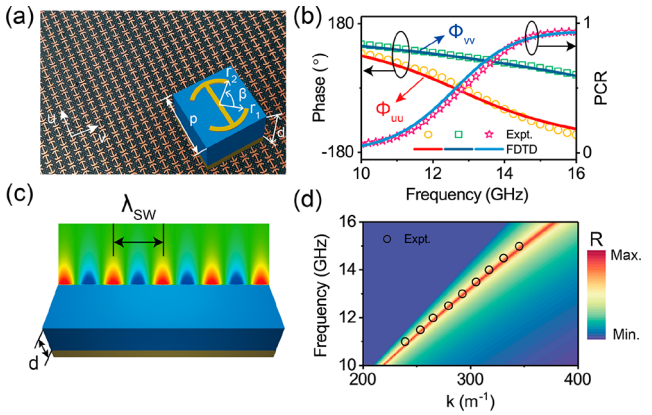

Figure 2. Characterizations of the proposed PB meta-atoms and plasmonic metal. (a) Image of part of the fabricated PB meta-atom array composed of the bent copper H-shaped resonator and a copper film that are separated by a thin dielectric spacer ($\varepsilon_r = 3$). Here, $p = 3.0$ mm, $d = 2$ mm, $r_1 = 1.1$ mm, $r_2 = 1.3$ mm, and $\beta = 90°$. (b) Spectra of reflection phase (Φ_{uu} and Φ_{vv}) and PCR of the designed meta-atoms obtained by full wave simulations and experiments. (c) Structural schematic and eigen SW field pattern (at 12 GHz) of the designed plasmonic metal consisting of a 2 mm thick dielectric spacer ($\varepsilon_r = 3$) capped on copper film. (d) Dispersion relation of the eigen SWs supported by the plasmonic metal shown in (c), based on numerical calculations (color map: reflectance spectra versus parallel wavevector and frequency) and near-field measurements (dots).

spin can successfully satisfy the perfect wavevector matching condition and thus result in the in-plane near-field scattering.

Consider first the simplest case that the phase gradient $\vec{\xi}^{\sigma} = \nabla\Phi^{\sigma} = \sigma(\xi_x\hat{x} + \xi_y\hat{y})$ provided by the metasurface is a constant vector. Under the excitation of a SW beam exhibiting a wavevector $\vec{k}_{SW}^{\,in}$, Huygens' principle analyses show that the beam formed by interference of waves scattered by the metasurface must exhibit a tangential wavevector $\vec{k}^{s}$:

$$\vec{k}^{s} = \vec{k}_{SW}^{\,in} + \vec{\xi}^{\sigma} \tag{1}$$

In order to make such a generated "beam" still a SW flowing on the surface, the following constraint should also be satisfied:

$$|\vec{k}^{s}| = k_{SW} \tag{2}$$

It is thus clear that only one of two anomalous modes (e.g., $\sigma = 1$) can satisfy eq 2, since the phase gradients obtained by two anomalous modes are opposite (see section B of the Supporting Information).

We extend our discussions to more generic cases where the metasurface does not exhibit a constant phase gradient vector everywhere and thus can exhibit a more generic SW-manipulation function other than beam bending. Assuming that we would like to locally bend the incident SW, originally flowing to the x direction, to an in-plane angle $\theta_r(x,y)$ at the position (x, y) on the metasurface (see Figure 1b), we can easily derive from eqs 1 and 2 the required phase gradient factors ξ_x and ξ_y for the metasurface at this particular point:

$$\begin{cases} \xi_x(x, y) = -k_{SW} + k_{SW}\cos\theta_r(x, y) \\ \xi_y(x, y) = k_{SW}\sin\theta_r(x, y) \end{cases} \tag{3}$$

These phase gradient functions, $\vec{\xi}(x, y)$, can then help us retrieve the phase distribution encoded by the metasurface (see more details in section F of the Supporting Information):

$$\Phi(x, y) = \int \xi_x(x, y)\,dx + \int \xi_y(x, y)\,dy - \iint \frac{\partial \xi_x(x, y)}{\partial y}\,dx\,dy \tag{4}$$

in order to reconstruct the desired SW wavefront (see Figure 1c). We finally derive from the PB theory the orientation-angle distribution of meta-atoms: $\alpha(x, y) = \Phi_{MS}(x, y)/2$, which can be used to construct our meta-device.

Without losing generality, we choose the microwave regime to demonstrate our concept. Figure 2a depicts the proposed PB meta-atom in a metal−insulator−metal (MIM) configuration, consisting of a copper resonator and a copper thin film separated by a 2 mm thick F4B dielectric spacer ($\varepsilon_r = 3$). We first study the reflection property of such anisotropic unit structures under normal incidence, which is described by a Jones matrix $R = \begin{pmatrix} r_{uu} & 0 \\ 0 & r_{vv} \end{pmatrix}$ with u and v denoting two principle axes of the meta-atom. Here, the off-diagonal terms of the Jones matrix are strictly zero considering that the adopted meta-atom possesses a mirror symmetry. The top resonator consists of two metallic arcs connected by a central metal bar, which exhibits enough free parameters to tune the anisotropy in optical responses. Shined by the impinging PWs, strong magnetic resonances will be induced inside the PB meta-atoms. The thickness of dielectric spacer determines the coupling strength between two metallic layers, eventually influencing the frequency dispersion of reflection phase.[45] After careful optimizations, we fix the structural details of our meta-atom, and then fabricate out a sample containing a periodic array of such meta-atoms. We measure the reflection-phase spectra (Φ_{uu} and Φ_{vv}) of the sample and depict them in Figure 2b, compared with those obtained with finite-difference-time-domain (FDTD) simulations. We find that the phase difference $\Phi_{uu} - \Phi_{vv}$ increases continuously from 28° to 147° as the frequency changes from 10 to 16 GHz. Meanwhile, due to the presence of a metal on the back, the meta-atom can reflect impinging EM waves perfectly, and we have $|r_{uu}|$ and $|r_{vv}|$ both close to 100%. The polarization conversion ratio (PCR) of the meta-atom (defined as $|(r_{uu} - r_{vv})/2|^2$), which is an important parameter to characterize the efficiency of anomalous-mode generation, can be calculated based on the measured reflection coefficients. As shown in Figure 2b, we find that the PCR of our meta-atom increases continuously from 0.05 to 0.92 as frequency changes from 10 to 16 GHz.

We also design a "plasmonic metal" to support eigen SWs in the microwave regime. To avoid causing undesired scatterings, the "plasmonic metal" is simply composed of a metallic thin film and a dielectric spacer of the same thickness as that of the PB meta-atom (see Figure 2c). Dispersion relation of eigen SWs supported by such a "plasmonic metal" is analytically computed employing the transfer matrix method, which is in nice agreement with our experimental measurements (see Figure 2d) based on near-field scanning technique.[34]

UNIDIRECTIONAL IN-PLANE DEFLECTION OF SWS

We proceed to experimentally demonstrate a simple SW wavefront engineering effect based on PB metasurface, i.e., the unidirectional deflection of SW. Specifically, as a SW beam flows across the metasurface along x direction, we expect that the SW beam is bent to a predesigned angle θ_r according to eq 3 (see Figure 3a). Phase distribution of such a PB metasurface can be easily derived from eq 4 as

$$\Phi(x, y) = k_{SW}\cos\theta_r x + k_{SW}\sin\theta_r y - k_{SW}x \tag{5}$$

https://doi.org/10.1021/acsphotonics.2c02009
ACS Photonics 2023, 10, 2423−2431

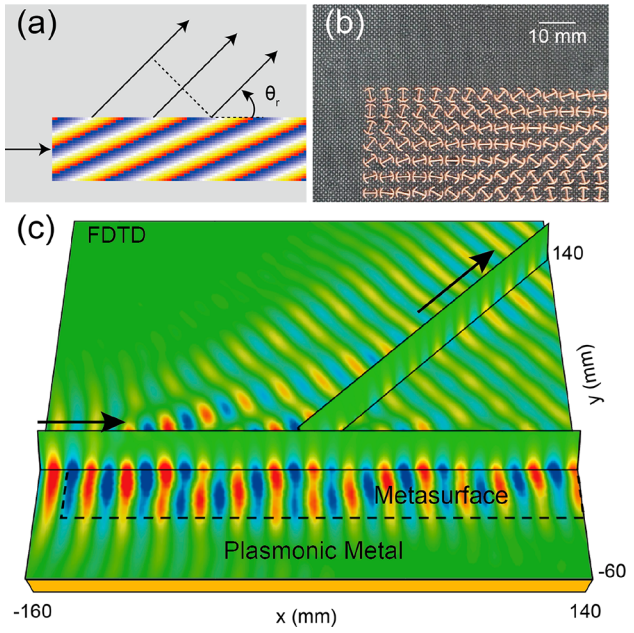

Figure 3. Unidirectional in-plane deflection of SW by PB metasurface. (a) Schematic of the SW deflection by metasurface with a constant phase gradient $\vec{\xi} = -0.293k_{SW}\hat{x} + 0.707k_{SW}\hat{y}$. (b) Image of part of the fabricated sample of our meta-device, which consists of the PB metasurface and plasmonic metal. (c) FDTD simulated electric field Re(E_z) distributions above the meta-device under the excitation of SWs at 12 GHz.

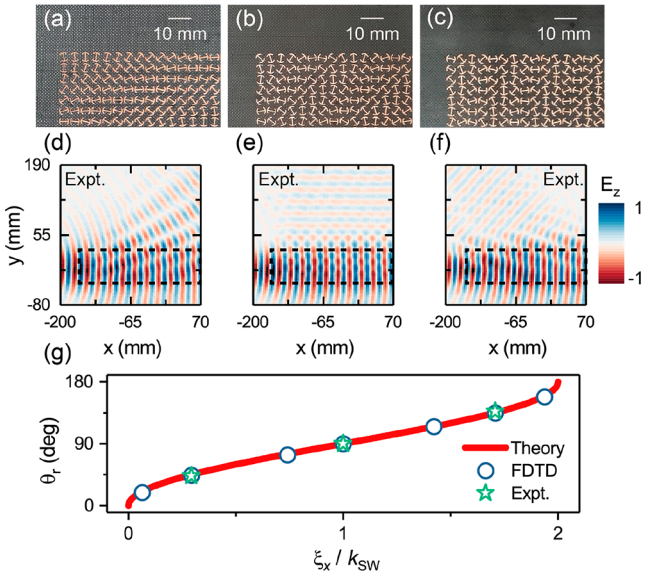

Figure 4. Verification of unidirectional in-plane of SW covering angle range of $0° < \theta_r < 180°$. (a–c) Pictures of three fabricated samples with different phase gradients $\vec{\xi}_1 = -0.293k_{SW}\hat{x} + 0.707k_{SW}\hat{y}$ (same to that in Figure 3), $\vec{\xi}_2 = -k_{SW}\hat{x} + k_{SW}\hat{y}$ and $\vec{\xi}_3 = -1.707k_{SW}\hat{x} + 0.707k_{SW}\hat{y}$, which will deflect the incident SW to the angle $\theta_{r1} = 45°$, $\theta_{r2} = 90°$, and $\theta_{r3} = 135°$, respectively. (d–f) Experimental measured Re(E_z) field distribution on the x–y plane with a distance 3 mm above the meta-devices. (g) Deflection angle of SW vs the phase gradient (ξ_x) of the adopted metasurfaces. Here, the frequency is set at 12 GHz.

from which the orientation angle distribution $\alpha(x, y)$ of our meta-atoms is known. Here, the term $-k_{SW}x$ in eq 5 is responsible for compensating the accumulated phase of the SW propagating along the metasurface. We therefore design and fabricate a sample consisting of the PB metasurface with meta-atoms arranged following the $\alpha(x, y)$ distribution and a "plasmonic metal" connected together, as shown in Figure 3b. Choosing the working frequency as 12 GHz, we find that our "plasmonic metal" supports an eigen SW with $k_{SW} = 1.07k_0$. The PB metasurface is composed of a series of identical PB meta-atoms with orientation angles varying with constant steps of $\Delta\alpha_x = -7°$ and $\Delta\alpha_y = +17°$ (here the sign "+" and "−" represent anticlockwise and clockwise rotation, respectively) along $+x$ and $+y$ directions, providing a phase gradient vector of $\vec{\xi} = -0.293k_{SW}\hat{x} + 0.707k_{SW}\hat{y}$ as desired. Here, we set the bending angle of SW at 12 GHz as $\theta_r = 45°$.

We first perform FDTD simulation to study the scattered field pattern as a SW beam passes through the metasurface. As depicted in Figure 3c, the simulated near-field Re(E_z) distribution clearly shows that the incident SW is efficiently deflected by the PB metasurface to the predesigned direction. For a metasurface with a long-enough length, we find that eventually almost all impinging SW can be deflected to the $\theta_r = 45°$ direction (about 93% efficiency in the present case). On the other hand, only a small portion of incident energy is scattered to the far field (here about 7%), which can be further reduced via optimizing the impedance difference between the meta-device and the plasmonic metal. Similar to meta-devices studied elsewhere,[46] as the frequency changes, the deflection efficiency of our meta-device will exhibit certain differences with respect to that at the optimized working frequency, considering that the dispersion of the system's impedance will affect the radiation loss.

We next fabricate the sample and employ the near-field mapping technique to experimentally verify our theoretical predictions. The meta-devices are fabricated based on the standard printed circuit board technology. In practical measurements, we adopt an additional meta-coupler to launch SWs under the illumination of a plane wave radiated from a horn antenna.[47] Exciting a SW beam to flow on the left-sided plasmonic metal, we employed a monopole antenna to scan the distribution of electric field E_z (with both amplitude and phase) on the x–y plane 3 mm above the sample. As shown in Figure 4d, the experimentally measured Re(E_z) pattern is in nice agreement with the simulated one (Figure 3c). We continue to experimentally demonstrate SW deflections to more angles inside [0°, 180°] via constructing PB metasurfaces with appropriate phase distributions according to eq 5. Figure 4a–c depicts the pictures of three fabricated sample phase distributions exhibiting different phase gradient vectors, i.e., $\vec{\xi}_1 = -0.293k_{SW}\hat{x} + 0.707k_{SW}\hat{y}$, $\vec{\xi}_2 = -k_{SW}\hat{x} + k_{SW}\hat{y}$ and $\vec{\xi}_3 = -1.707k_{SW}\hat{x} + 0.707k_{SW}\hat{y}$, which can deflect the impinging SW to the angles of $\theta_{r1} = 45°$, $\theta_{r2} = 90°$, and $\theta_{r3} = 135°$ at 12 GHz, respectively. To verify our theoretical predictions, we perform near-field scanning measurements to map the Re(E_z) distributions on the surfaces of three samples, as the same SW beams are excited on plasmonic metals to flow across these metasurfaces. As shown in Figure 4d–f, we find that the incident SWs are scattered to the angles of $\theta_{r1} \approx 44.0°$, $\theta_{r2} \approx 90°$, and $\theta_{r3} \approx 137°$ after passing through these metasurfaces, agreeing well with our theoretical expectations. In fact, we have designed more PB metasurfaces with different phase gradient vectors $\vec{\xi}$ and numerically demonstrate that these metasurfaces can deflect incident SW beams to different angles covering the whole region of $0° < \theta_r < 180°$, as depicted in Figure 4g. We can also easily realize metasurfaces to deflect the impinging SW beam to angles within the region [−180°, 0°], simply through changing the

https://doi.org/10.1021/acsphotonics.2c02009
ACS Photonics 2023, 10, 2423−2431

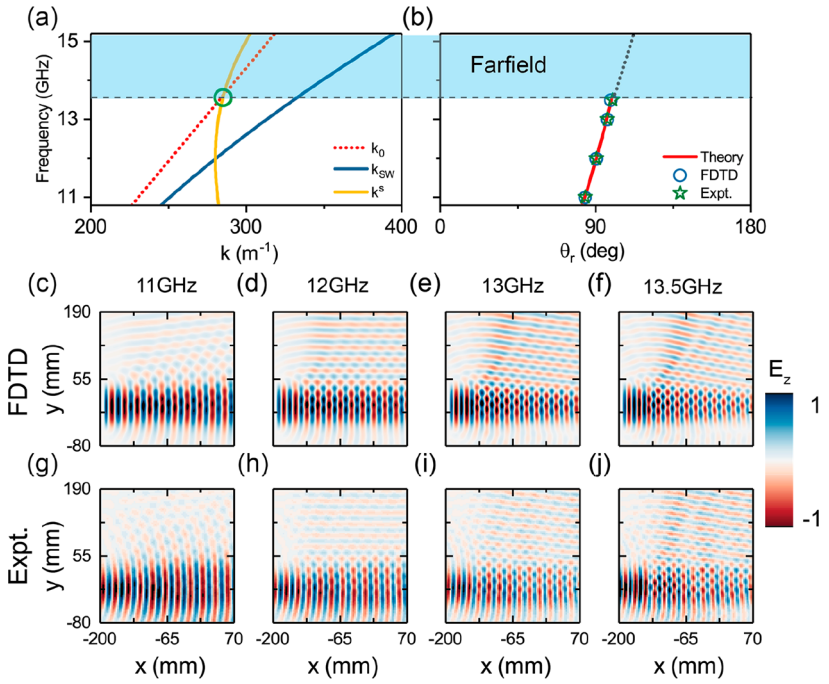

Figure 5. Verification of broadband SW deflection by PB metasurface. (a) In-plane wavevectors of the eigen SWs and scattered driven SWs (i.e., k_{SW} and $|\hat{k}^s| = |\hat{k}_{SW} + \vec{\xi}|$) by the metasurface shown in Figure 4b. (b) The deflection angle θ_r as the function of frequency. (g–j) Experimentally measured and (c–f) FDTD simulated Re(E_z) field distributions on x–y plane with a distance of 3 mm above the meta-device at 11, 12, 13, and 13.5 GHz.

orientation-angle distribution along the y direction (see section C of the Supporting Information).

We find that PCRs of constitutional meta-atoms play very important roles in the SW manipulations. Since the amplitude of anomalously scattered wave is proportional to the PCR of a meta-atom, varying the PCR can control the amplitude of locally scattered wave and thus reduce decay rate of the SW beam. Inspired by our previous works on SW-PW radiation manipulations by PB metasurface,[47] we adopted the similar strategy to utilize low-PCR meta-atoms (PCR = 0.3 at 12 GHz) to construct our PB metasurface, in order to minimize the decay rate of the impinging SW as it passes through the meta-device and thus construct a SW beam with a nearly flat wavefront. For comparison, we also design a series of meta-atoms exhibiting distinct PCR values (e.g., 0.41, 0.74, and 0.94 at the target frequency) as building components to construct three PB meta-devices with the same phase gradient vectors $\vec{\xi}_1 = -0.293k_{SW}\hat{x} + 0.707k_{SW}\hat{y}$. Full wave simulations on these samples demonstrate that the intensity of the bended SW beam is proportional to the PCR value of the constitutional meta-atom, offering us the capabilities of independently controlling both scattered phase and amplitude of SWs at the deep-subwavelength scale. More details can be found in section D of the Supporting Information.

We now investigate the working bandwidth of our meta-devices. Owing to the dispersionless nature of geometric phases, phase gradient vectors provided by these PB metasurfaces are all independent of frequency. Meanwhile, the eigen wavevector of SW gradually varies with frequency, following the dispersion relation depicted in Figure 2d. Therefore, wavevector-matching (i.e., $|\vec{k}^s| = |\vec{k}_{SW} + \vec{\xi}| = k_{SW}$) can only be strictly satisfied at the central working frequency. As the frequency changes, the governed principle of in-plane scattering of SW will be replaced by the quasi wavevector matching condition (i.e., $|\vec{k}^s| = |\vec{k}_{SW} + \vec{\xi}| \approx k_{SW}$). Figure 5a depicts the wavevector spectra of scattering wave (i.e., k^s) and eigen SW (i.e., k_{SW}) modulated by the PB metasurface with the phase gradient $\vec{\xi}_2 = -k_{SW}\hat{x} + k_{SW}\hat{y}$. It is noted that the tangential wavevector of scattered waves always satisfies $|\vec{k}^s| > k_0$ at the frequency less than 13.7 GHz, which is the signature of in-plane SW scattering, and the direction of in-plane scattered SW will be governed by the equation $\theta_r = \cos^{-1}\left(\frac{k_{SW} + \xi_x}{k_{SW}}\right)$. Here, the sign of ξ_x should be different from that of k_{SW}. While the metasurface compensates an opposite wavevector for the impinging SW, it may generate the deflected SW propagating along θ_r. It should be emphasized that, although ξ_y doesn't exist in eq 6, it is still an indispensable component to help satisfy the condition of in-plane scattering, i.e., perfect (or quasi) wavevector matching condition (see more details in section E of the Supporting Information). To verify the broadband performance of in-plane SW scattering, we have adopted the same near-field scanning technique to characterize the near field Re(E_z) at several representative frequencies (i.e., 11, 12, 13, and 13.5 GHz), as shown in Figure 5g–j. Obviously, the impinging SWs are anomalously deflected along different directions in the 2D plane. All these behaviors of broadband near-field manipulations are further demonstrated by the full wave simulations (see Figure 5c–f). As shown in Figure 5b, both the simulated and measured in-plane scattering angle of the outgoing SWs generated by the PB metasurface coincide with the theoretical prediction. Meanwhile, at the frequency above 13.7 GHz, the tangential wavevector of scattering wave satisfies $|\vec{k}_s| < k_0$, implying that the impinging SWs will be decoupled to far-field free space.[47]

COMPLEX IN-PLANE WAVEFRONT RESHAPING OF SWS

In this section, we further employ the proposed strategy to achieve more complicated near-field wavefront reshaping by metasurface. The first meta-device is constructed to focus the SWs at the predefined focal point on the 2D plane, as depicted in

https://doi.org/10.1021/acsphotonics.2c02009
ACS Photonics 2023, 10, 2423–2431

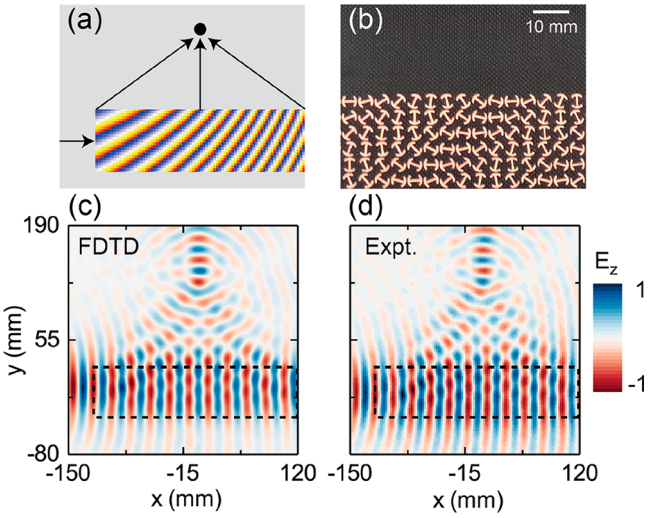

Figure 6. In-plane focusing of SWs by PB metasurface. (a) The schematic of SW focusing at the focal point F. Here, the color map represents the phase distribution of PB metasurface described by eq 7. (b) Image of part of the fabricated meta-device. (c, d) FDTD simulated and experimentally measured Re(E_z) field distributions on the x−y plane, with a distance of 3 mm above the sample. Here, the frequency is set at 12 GHz.

Figure 6a. The phase distribution of the PB meta-device should satisfy the following equation (see derivation in section F of the Supporting Information):

$$\Phi_{\text{focus}}(x, y) = k_{\text{SW}}(-x - \sqrt{x^2 + (F - y)^2}) \quad (6)$$

where F = 125 mm is the focal length. Following eq 6, we can retrieve the orientation angle distribution $\alpha(x, y) = \Phi_{\text{focus}}(x, y)/2$ of the PB meta-atoms and thus guide the fabrication of the desired meta-device based on the same building block depicted in Figure 2. Figure 6b shows the image of part of the fabricated sample including the metasurface (240 × 75 mm^2) and the surrounding plasmonic metal. We then performed the near-field mapping experiment to obtain the Re(E_z) field distribution on an x−y plane 3 mm away from the meta-devices under the excitation of SWs traveling along x direction (see Figure 6d). Obviously, the incident SWs are efficiently focused to the focal point on the plasmonic metal, showing a good agreement with simulation results as depicted in Figure 6c.

Finally, we further achieve the generation of the non-diffraction SW beams such as near-field Bessel beam and Airy beam by metasurfaces, as schematically depicted in Figures 7a,d. We find that the phase distributions for the two PB meta-devices can be described, respectively, by the following equations (see derivation in section F of the Supporting Information):

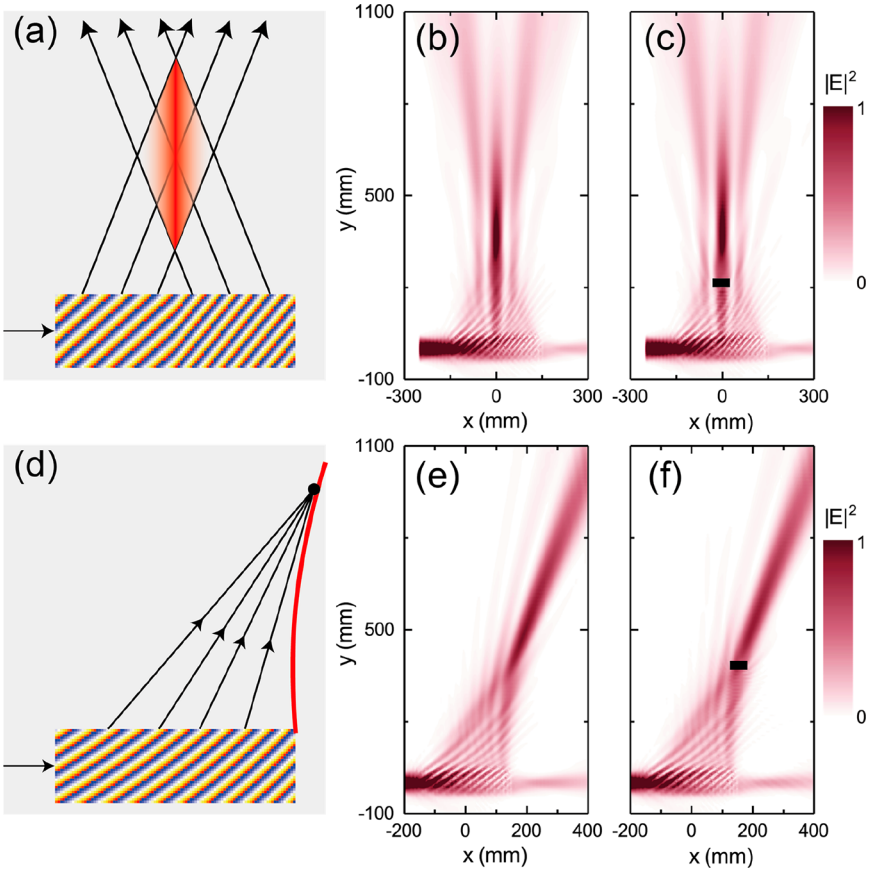

Figure 7. Nondiffraction SW beams generations. (a, d) Schematics of generating Bessel beam and Airy beam by PB metasurfaces. (b, e) FDTD simulated E-field distributions of Bessel beam and Airy beam on the x−y plane with a distance of 3 mm above the meta-devices. (c, f) Characterizations of the self-healing effect for these two generated nondiffraction beams. Here, the frequency is set at 12 GHz.

https://doi.org/10.1021/acsphotonics.2c02009
ACS Photonics 2023, 10, 2423−2431

$$\Phi_{\text{Bessel}}(x, y) = \begin{cases} k_{\text{SW}}(-x + x\cos\theta_0 + y\sin\theta_0), & x < 0 \\ k_{\text{SW}}(-x - x\cos\theta_0 + y\sin\theta_0), & x \geq 0 \end{cases} \tag{7}$$

$$\Phi_{\text{Airy}}(x, y) = -k_{\text{SW}}x + \frac{k_{\text{SW}}}{2}\left(y - \sqrt{y^2 - \frac{x}{a}}\right) \times \sqrt{1 - 4ax + 8a^2y\left(y + \sqrt{y^2 - \frac{x}{a}}\right)} + \frac{k_{\text{SW}}}{4a}\,\text{arcsinh}\left[2a\left(y + \sqrt{y^2 - \frac{x}{a}}\right)\right], \quad (x < 0,\ y < 0) \tag{8}$$

where $\theta_0 = 10°$, $a = 0.24\ \text{m}^{-1}$, and $k_{\text{SW}} = 1.07k_0$ at the central frequency 12 GHz. The total size for both metasurfaces is 300 × 90 mm^2, which are composed of 100 × 30 PB meta-atoms and the "plasmonic metal". FDTD simulations are performed to verify our predictions. In Figure 7b, it is clearly shown that a long-distance nondiffraction beam trajectory appears after SWs pass through the designed metasurface. To exhibit the self-healing property of near-field Bessel beam, an obstacle (i.e., a 25 × 10 mm^2 rectangular hole) is added at the position of (x = 0 mm, y = 200 mm) on plasmonic metal, which exactly locates on the propagation path of near-field Bessel beam. Figure 7c shows that such an obstacle will not influence the in-plane propagation of SW Bessel beam, confirming its self-healing behavior. Another PB metasurface also exhibits its capability to convert the input SW beam into the nondiffraction Airy beam, as demonstrated in Figure 7e,f. It is clearly demonstrated that the desired SW Airy beam with the self-bending and nonspreading lobes is launched after SWs pass through the designed metasurface. Even while encountering the same 25 × 10 mm^2 rectangular hole, the near-field Airy beam can still heal by itself, as shown in Figure 7f. Here, size and shape (within a certain variation range) of the air hole will not influence the self-healing property of the generated nondiffraction beams.[48,49]

CONCLUSIONS

We propose a new scheme to design PB meta-devices for realizing the in-plane wavefront engineering of SWs. The meta-device can provide an additional wavevector to impinging SWs and thus locally change their propagation directions, building up the predefined SW wavefront. To prove our idea, we design and fabricate a set of PB meta-devices working in the microwave regime that can achieve various near-field controls such as SW beam deflection, near-field focusing, SW Bessel beam and Airy beam generation. Compared with the conventional approaches (e.g., optical elements or Bragg devices), our scheme shows intriguing properties of single-mode operation, high efficiency, subwavelength modulation, easy integration, and so on. In particular, the perfect wavevector matching condition for SW manipulations can be well satisfied in the proposed PB meta-devices. Such a concept is quite generic that can be further developed to high frequency regimes (see numerical demonstration in section G of the Supporting Information). Our findings may inspire many potential applications in on-chip integrated optics, e.g., on-chip switches, plasmonic tweezers, near-field imaging, optical computing, and so on.

ASSOCIATED CONTENT

Supporting Information

The Supporting Information is available free of charge at https://pubs.acs.org/doi/10.1021/acsphotonics.2c02009.

Additional experimental details and supporting references (PDF)

AUTHOR INFORMATION

Corresponding Authors

Shulin Sun − *Shanghai Engineering Research Center of Ultra-Precision Optical Manufacturing, Department of Optical Science and Engineering, School of Information Science and Technology, Fudan University, Shanghai 200433, China; Yiwu Research Institute of Fudan University, Yiwu City 322000 Zhejiang, China;* orcid.org/0000-0003-3046-1142; Email: sls@fudan.edu.cn

Lei Zhou − *State Key Laboratory of Surface Physics and Key Laboratory of Micro and Nano Photonic Structures (Ministry of Education), Fudan University, Shanghai 200433, China; Collaborative Innovation Center of Advanced Microstructures, Nanjing 210093, China*; Email: phzhou@fudan.edu.cn

Authors

Weikang Pan − *Shanghai Engineering Research Center of Ultra-Precision Optical Manufacturing, Department of Optical Science and Engineering, School of Information Science and Technology, Fudan University, Shanghai 200433, China; Yiwu Research Institute of Fudan University, Yiwu City 322000 Zhejiang, China*

Zhuo Wang − *State Key Laboratory of Surface Physics and Key Laboratory of Micro and Nano Photonic Structures (Ministry of Education), Fudan University, Shanghai 200433, China*

Yizhen Chen − *Shanghai Engineering Research Center of Ultra-Precision Optical Manufacturing, Department of Optical Science and Engineering, School of Information Science and Technology, Fudan University, Shanghai 200433, China*

Xiaoying Zheng − *State Key Laboratory of Surface Physics and Key Laboratory of Micro and Nano Photonic Structures (Ministry of Education), Fudan University, Shanghai 200433, China*

Shiqing Li − *Shanghai Engineering Research Center of Ultra-Precision Optical Manufacturing, Department of Optical Science and Engineering, School of Information Science and Technology, Fudan University, Shanghai 200433, China*

Xinzhang Tian − *Shanghai Engineering Research Center of Ultra-Precision Optical Manufacturing, Department of Optical Science and Engineering, School of Information Science and Technology, Fudan University, Shanghai 200433, China*

Qiong He − *State Key Laboratory of Surface Physics and Key Laboratory of Micro and Nano Photonic Structures (Ministry of Education), Fudan University, Shanghai 200433, China; Collaborative Innovation Center of Advanced Microstructures, Nanjing 210093, China*

Complete contact information is available at: https://pubs.acs.org/10.1021/acsphotonics.2c02009

Author Contributions

#W.P. and Z.W. are cofirst authors.

Funding

This work was supported by National Key Research and Development Program of China (Nos. 2022YFA1404700, 2020YFA0710100, and 2017YFA0700201), National Natural Science Foundation of China (Nos. 11874118, 12221004, 91850101, 11734007, and 62192771), and Shanghai Science and Technology Committee (No. 20JC1414601).

Notes

The authors declare no competing financial interest.

REFERENCES

(1) Barnes, W. L.; Dereux, A.; Ebbesen, T. W. Surface Plasmon Subwavelength Optics. *Nature* **2003**, *424* (6950), 824−830.

(2) Pendry, J. B.; Martin-Moreno, L.; Garcia-Vidal, F. J. Mimicking Surface Plasmons with Structured Surfaces. *Science* **2004**, *305* (5685), 847−848.

(3) Maier, S. A. *Plasmonics: Fundamentals and Applications*; Springer Press, 2007.

(4) Pendry, J. B. Negative Refraction Makes a Perfect Lens. *Phys. Rev. Lett.* **2000**, *85* (18), 3966−3969.

(5) Fang, N.; Lee, H.; Sun, C.; Zhang, X. Sub-Diffraction-Limited Optical Imaging with a Silver Superlens. *Science* **2005**, *308* (5721), 534−537.

(6) Anker, J. N.; Hall, W. P.; Lyandres, O.; Shah, N. C.; Zhao, J.; Van Duyne, R. P. Biosensing with Plasmonic Nanosensors. *Nat. Mater.* **2008**, *7* (6), 442−453.

(7) Zhang, S.; Bao, K.; Halas, N. J.; Xu, H.; Nordlander, P. Substrate-Induced Fano Resonances of a Plasmonic Nanocube: A Route to Increased-Sensitivity Localized Surface Plasmon Resonance Sensors Revealed. *Nano Lett.* **2011**, *11* (4), 1657−1663.

(8) Zhang, X.; Cui, T. J. Contactless Glucose Sensing at Sub-Micromole Level Using a Deep-Subwavelength Decimeter-Wave Plasmonic Resonator. *Laser Photon. Rev.* **2022**, *16* (10), 2200221.

(9) Bergman, D. J.; Stockman, M. I. Surface Plasmon Amplification by Stimulated Emission of Radiation: Quantum Generation of Coherent Surface Plasmons in Nanosystems. *Phys. Rev. Lett.* **2003**, *90* (2), 027402.

(10) Oulton, R. F.; Sorger, V. J.; Zentgraf, T.; Ma, R. M.; Gladden, C.; Dai, L.; Bartal, G.; Zhang, X. Plasmon Lasers at Deep Subwavelength Scale. *Nature* **2009**, *461* (7264), 629−632.

(11) Azzam, S. I.; Kildishev, A. V.; Ma, R.-M.; Ning, C.-Z.; Oulton, R.; Shalaev, V. M.; Stockman, M. I.; Xu, J.-L.; Zhang, X. Ten Years of Spasers and Plasmonic Nanolasers. *Light Sci. Appl.* **2020**, *9* (1), 90.

(12) Bozhevolnyi, S. I.; Volkov, V. S.; Devaux, E.; Laluet, J. Y.; Ebbesen, T. W. Channel Plasmon Subwavelength Waveguide Components Including Interferometers and Ring Resonators. *Nature* **2006**, *440* (7083), 508−511.

(13) Wei, H.; Wang, Z.; Tian, X.; Käll, M.; Xu, H. Cascaded Logic Gates in Nanophotonic Plasmon Networks. *Nat. Commun.* **2011**, *2* (1), 387.

(14) Meng, Y.; Chen, Y.; Lu, L.; Ding, Y.; Cusano, A.; Fan, J. A.; Hu, Q.; Wang, K.; Xie, Z.; Liu, Z.; Yang, Y.; Liu, Q.; Gong, M.; Xiao, Q.; Sun, S.; Zhang, M.; Yuan, X.; Ni, X. Optical Meta-Waveguides for Integrated Photonics and Beyond. *Light Sci. Appl.* **2021**, *10* (1), 235.

(15) Palomba, S.; Novotny, L. Nonlinear Excitation of Surface Plasmon Polaritons by Four-Wave Mixing. *Phys. Rev. Lett.* **2008**, *101* (5), 056802.

(16) Kauranen, M.; Zayats, A. V. Nonlinear Plasmonics. *Nat. Photonics* **2012**, *6* (11), 737−748.

(17) Shi, J.; Li, Y.; Kang, M.; He, X.; Halas, N. J.; Nordlander, P.; Zhang, S.; Xu, H. Efficient Second Harmonic Generation in a Hybrid Plasmonic Waveguide by Mode Interactions. *Nano Lett.* **2019**, *19* (6), 3838−3845.

(18) Hohenau, A.; Krenn, J. R.; Stepanov, A. L.; Drezet, A.; Ditlbacher, H.; Steinberger, B.; Leitner, A.; Aussenegg, F. R. Dielectric Optical Elements for Surface Plasmons. *Opt. Lett.* **2005**, *30* (8), 893.

(19) Devaux, E.; Laluet, J.-Y.; Stein, B.; Genet, C.; Ebbesen, T.; Weeber, J.-C.; Dereux, A. Refractive Micro-Optical Elements for Surface Plasmons: From Classical to Gradient Index Optics. *Opt. Express* **2010**, *18* (20), 20610.

(20) González, M. U.; Weeber, J. C.; Baudrion, A. L.; Dereux, A.; Stepanov, A. L.; Krenn, J. R.; Devaux, E.; Ebbesen, T. W. Design, near-Field Characterization, and Modeling of 45° Surface-Plasmon Bragg Mirrors. *Phys. Rev. B* **2006**, *73* (15), 155416.

(21) Li, L.; Li, T.; Wang, S. M.; Zhang, C.; Zhu, S. N. Plasmonic Airy Beam Generated by In-Plane Diffraction. *Phys. Rev. Lett.* **2011**, *107* (12), 126804.

(22) Li, L.; Li, T.; Wang, S. M.; Zhu, S. N. Collimated Plasmon Beam: Nondiffracting versus Linearly Focused. *Phys. Rev. Lett.* **2013**, *110* (4), 046807.

(23) Chen, Y.-G.; Chen, Y.-H.; Li, Z.-Y. Direct Method to Control Surface Plasmon Polaritons on Metal Surfaces. *Opt. Lett.* **2014**, *39* (2), 339.

(24) Chen, Y.-G.; Yang, F.-Y.; Liu, J.; Li, Z.-Y. Broadband Focusing and Demultiplexing of Surface Plasmon Polaritons on Metal Surface by Holographic Groove Patterns. *Opt. Express* **2014**, *22* (12), 14727.

(25) Yu, N.; Genevet, P.; Kats, M. a; Aieta, F.; Tetienne, J. P.; Capasso, F.; Gaburro, Z. Light Propagation with Phase Discontinuities: Generalized Laws of Reflection and Refraction. *Science* **2011**, *334* (6054), 333−337.

(26) Sun, S.; He, Q.; Xiao, S.; Xu, Q.; Li, X.; Zhou, L. Gradient-Index Meta-Surfaces as a Bridge Linking Propagating Waves and Surface Waves. *Nat. Mater.* **2012**, *11* (5), 426−431.

(27) Minovich, A.; Klein, A. E.; Janunts, N.; Pertsch, T.; Neshev, D. N.; Kivshar, Y. S. Generation and Near-Field Imaging of Airy Surface Plasmons. *Phys. Rev. Lett.* **2011**, *107* (11), 116802.

(28) Epstein, I.; Arie, A. Arbitrary Bending Plasmonic Light Waves. *Phys. Rev. Lett.* **2014**, *112* (2), 023903.

(29) Kou, S. S.; Yuan, G.; Wang, Q.; Du, L.; Balaur, E.; Zhang, D.; Tang, D.; Abbey, B.; Yuan, X.-C.; Lin, J. On-Chip Photonic Fourier Transform with Surface Plasmon Polaritons. *Light Sci. Appl.* **2016**, *5* (2), e16034.

(30) Wang, Y.; Min, C.; Zhang, Y.; Feng, F.; Si, G.; Li, L.; Yuan, X. Drawing Structured Plasmonic Field with On-Chip Metalens. *Nanophotonics* **2022**, *11* (9), 1969−1976.

(31) Pors, A.; Nielsen, M. G.; Bernardin, T.; Weeber, J. C.; Bozhevolnyi, S. I. Efficient Unidirectional Polarization-Controlled Excitation of Surface Plasmon Polaritons. *Light Sci. Appl.* **2014**, *3*, e197.

(32) Lee, S.-Y.; Kim, K.; Kim, S.-J.; Park, H.; Kim, K.-Y.; Lee, B. Plasmonic Meta-Slit: Shaping and Controlling near-Field Focus. *Optica* **2015**, *2* (1), 6.

(33) Mühlenbernd, H.; Georgi, P.; Pholchai, N.; Huang, L.; Li, G.; Zhang, S.; Zentgraf, T. Amplitude- and Phase-Controlled Surface Plasmon Polariton Excitation with Metasurfaces. *ACS Photonics* **2016**, *3* (1), 124−129.

(34) Sun, W.; He, Q.; Sun, S.; Zhou, L. High-Efficiency Surface Plasmon Meta-Couplers: Concept and Microwave-Regime Realizations. *Light Sci. Appl.* **2016**, *5* (1), e16003.

(35) Wintz, D.; Ambrosio, A.; Zhu, A. Y.; Genevet, P.; Capasso, F. Anisotropic Surface Plasmon Polariton Generation Using Bimodal V-Antenna Based Metastructures. *ACS Photonics* **2017**, *4* (1), 22−27.

(36) Duan, J.; Guo, H.; Dong, S.; Cai, T.; Luo, W.; Liang, Z.; He, Q.; Zhou, L.; Sun, S. High-Efficiency Chirality-Modulated Spoof Surface Plasmon Meta-Coupler. *Sci. Rep.* **2017**, *7* (1), 1354.

(37) Ding, F.; Deshpande, R.; Bozhevolnyi, S. I. Bifunctional Gap-Plasmon Metasurfaces for Visible Light: Polarization-Controlled Unidirectional Surface Plasmon Excitation and Beam Steering at Normal Incidence. *Light Sci. Appl.* **2018**, *7* (4), 17178.

(38) Xu, Q.; Zhang, X.; Wei, M.; Ren, G.; Xu, Y.; Li, Y.; Wang, H.; Ouyang, C.; Han, J.; Zhang, W. Efficient Metacoupler for Complex Surface Plasmon Launching. *Adv. Opt. Mater.* **2018**, *6* (5), 1701117.

(39) Jin, J.; Li, X.; Guo, Y.; Pu, M.; Gao, P.; Ma, X.; Luo, X. Polarization-Controlled Unidirectional Excitation of Surface Plasmon Polaritons Utilizing Catenary Apertures. *Nanoscale* **2019**, *11* (9), 3952−3957.

(40) Li, S.; Wang, Z.; Dong, S.; Yi, S.; Guan, F.; Chen, Y.; Guo, H.; He, Q.; Zhou, L.; Sun, S. Helicity-Delinked Manipulations on Surface Waves and Propagating Waves by Metasurfaces. *Nanophotonics* **2020**, *9* (10), 3473−3481.

(41) Wang, Z.; Li, S.; Zhang, X.; Feng, X.; Wang, Q.; Han, J.; He, Q.; Zhang, W.; Sun, S.; Zhou, L. Excite Spoof Surface Plasmons with Tailored Wavefronts Using High-Efficiency Terahertz Metasurfaces. *Adv. Sci.* **2020**, *7* (19), 2000982.

https://doi.org/10.1021/acsphotonics.2c02009
ACS Photonics 2023, 10, 2423−2431

(42) Guan, F.; Sun, S.; Xiao, S.; He, Q.; Zhou, L. Scatterings from Surface Plasmons to Propagating Waves at Plasmonic Discontinuities. *Sci. Bull.* **2019**, *64* (12), 802−807.
(43) Huang, L.; Chen, X.; Muhlenbernd, H.; Li, G.; Bai, B.; Tan, Q.; Jin, G.; Zentgraf, T.; Zhang, S. Dispersionless Phase Discontinuities for Controlling Light Propagation. *Nano Lett.* **2012**, *12* (11), 5750−5755.
(44) Luo, W.; Xiao, S.; He, Q.; Sun, S.; Zhou, L. Photonic Spin Hall Effect with Nearly 100% Efficiency. *Adv. Opt. Mater.* **2015**, *3* (8), 1102−1108.
(45) Sun, S.; Yang, K. Y.; Wang, C. M.; Juan, T. K.; Chen, W. T.; Liao, C. Y.; He, Q.; Xiao, S.; Kung, W.-T.; Guo, G.-Y.; Zhou, L.; Tsai, D. P. High Efficiency Broadband Anomalous Reflection by Gradient Meta-Surfaces. *Nano Lett.* **2012**, *12* (12), 6223−6229.
(46) Hassanfiroozi, A.; Cheng, Y.-C.; Huang, S.-H.; Lin, Y.-T.; Huang, P.-S.; Shi, Y.; Wu, P. C. Toroidal-Assisted Generalized Huygens' Sources for Highly Transmissive Plasmonic Metasurfaces. *Laser Photon. Rev.* **2022**, *16* (6), 2100525.
(47) Pan, W.; Wang, Z.; Chen, Y.; Li, S.; Zheng, X.; Tian, X.; Chen, C.; Xu, N.; He, Q.; Zhou, L.; Sun, S. High-Efficiency Generation of Far-Field Spin-Polarized Wavefronts via Designer Surface Wave Meta-surfaces. *Nanophotonics* **2022**, *11* (9), 2025−2036.
(48) Ahmed, H.; Rahim, A. A.; Ali, M. M.; Maab, H. Symmetric Accelerating Beam Generation via All-Dielectric Metasurfaces. *RSC Adv.* **2020**, *10* (51), 30282−30288.
(49) Ahmed, H.; Rahim, A. A.; Maab, H.; Ali, M. M.; Naureen, S. Polarization Insensitive All-Dielectric Metasurfaces for the Ultraviolet Domain. *Opt. Mater. Express* **2020**, *10* (4), 1083−1091.

https://doi.org/10.1021/acsphotonics.2c02009
ACS Photonics 2023, 10, 2423−2431